Atomic holography with x rays

B. Adams, D. V. Novikov, T. Hiort, and G. Materlik
Hamburger Synchrotronstrahlungslabor HASYLAB am Deutschen Elektronen-Synchrotron DESY, D-22607 Hamburg, Germany

E. Kossel
II. Institut für Experimentalphysik, Universität Hamburg, Luruper Chaussee 149, D-22671 Hamburg, Germany
(Received 25 July 1997)

A theoretical treatment of atomic holography with x rays, taking into account the vectorial nature of electromagnetic waves is described. Direct and reciprocal holography are compared and put into the context of x-ray crystallography and the Kossel technique. The theoretical results are compared to experimental data on Cu_3Au. [S0163-1829(98)00713-9]

I. INTRODUCTION

Atomic holography, a technique very much akin to lensless Fourier transform holography,[1] was originally proposed by Szöke[2] for both electrons and x rays. The general problem of reconstructing three-dimensional objects from holographic data has already earlier been discussed by Wolf.[3] The electron variant of atomic holography is by now a well established technique for surface structure analysis.[4–10] Tegze and Faigel[11] realized the method of direct atomic x-ray holography and in parallel, Gog *et al.*[12] developed and proved experimentally the method of reciprocal atomic holography.

Both of these methods use the scattering of x rays to obtain information on the neighborhood of atoms of a specific species in a sample. In the direct method, these atoms are excited to x-ray fluorescence which is scattered from the neighbors so that in the far field, there is a slight angular modulation of the fluorescent radiation due to interference of the primary fluorescent wave with the scattered ones. In the reciprocal method, the direction of an ideally plane wave is scanned relative to the sample. Because this reference wave is scattered from the neighboring atoms and interferes with the scattered object waves, the local electrical field intensity that excites to fluorescence depends on the incidence angle. The fluorescence yield is then a measure of the exciting intensity. Therefore, in the reciprocal method, the detector is the fluorescing atom. In both, direct and reciprocal holography, the interference pattern is generated by fully coherent waves because the differences in optical path lengths are in the order of a few interatomic distances.

Although an atomic hologram could in principle be obtained from a small cluster, containing just the fluorescent atom and its immediate neighbors, real samples always contain many fluorescent atoms with like and similarly oriented neighborhoods. This makes no fundamental difference; the intensity measured at a large sample is simply proportional to what would be obtained from the small cluster. Therefore, the data set is always treated as if it had been obtained from a cluster with just one fluorescing atom. Atomic holography does not attempt to image the sample as a whole. In contrast to diffraction methods, atomic holography does not rely on any coherence between the emissions from different atoms. It is therefore well suited to the study of samples which have only rotational, but no translational order.

Far from absorption edges, only Thomson scattering is relevant. Interpretation of the data should be much more straightforward than in electron holography[13] because the Thomson scattering phase is isotropic. However, polarization averaging produces a strong anisotropy in the scattering phase of an equivalent scalar formalism (see Sec. II A). Due to the small cross section in the scattering of x rays from electrons, the interference signal is very weak in most cases, requiring long measuring times and high counting rates. An exception is the phenomenon of Kossel lines which were first observed[14] in 1934. Despite the weak scattering contribution from a single atom, the coherent superposition of scattered waves from many atoms in a crystalline sample gives a strong signal in certain crystallographic directions. The strength and width of the Kossel lines depends on the crystalline quality of the sample and the coherence of the illuminating wave, i.e., the fluorescence linewidth in the case of direct holography and the lateral coherence and monochromaticity in the case of reciprocal holography. The features in a holographic data set which change (i.e., sharpen) with the sample size contain diffractive contributions while the parts that are independent of the sample size consist of purely holographic data.

Simply put, the holographic information on long range order in a sample is contained in the Kossel lines while the short range order information can be found in the weak modulation between the Kossel lines—quite in analogy to the technique of crystal truncation rods.[15–18] The relation of reciprocal holography to direct holography is the same as the relation of the method of standing waves[19] to the method of standing waves in reverse.[20]

The holographic reconstruction procedure is essentially a reversal of waves; it is done numerically in the case of x rays and electrons. In addition to the images of the real atoms, ghost images may appear in single energy holograms.[7] They may be suppressed by the technique of multiple energy holography which has been applied for x rays[12] and for electrons.[8–10] Multiple energy holography is best done with the reciprocal method because there, the recording wavelength may be chosen quite freely—the x-ray energy only has to lie above the absorption edge of the detecting atomic species.

Conventional Gabor holography schemes,[21–23] extended to Å wavelengths do not reach atomic resolution, one reason (at least in the case of x rays) being that the interference pattern is recorded only in a relatively small solid angle, i.e., with a small numerical aperture. In atomic holography, either the radiation source (in the direct method) or the detector (in the reciprocal method) is inside the sample. Therefore, the interference pattern is recorded in a solid angle which may be as large as 4π, providing a resolution in the order of the wavelength.

There are already several theoretical and experimental articles which compare electron and x-ray holography and show the specific strengths of the methods.[13,24,25] In this paper, we will discuss direct and reciprocal x-ray holography, put them into the context of classical crystallographic methods and develop an intuitively simple but formally exact interpretation of the ghost images and their removal by multiple energy holography. We also show recent experimental results which are in good agreement with the theory.

II. THEORY

In the following treatment, we always assume the fluorescing atom—either as emitter in direct holography or as detector in reciprocal holography—to be in the coordinate origin. In reality, the sample contains a large number of such atoms, each of which may be the emitter of fluorescence. We treat the measured data as an incoherent superposition of the holograms produced by them. If all fluorescent atoms are located at structurally equivalent sites and their environments all have the same orientation in space, the measured hologram is the same as would be obtained from a sample with just one fluorescent atom. In the case of several structurally inequivalent sites for the fluorescing atoms, the reconstruction will show a superposition of all neighborhoods.

Although the source or the detector is inside the sample, the intensity of a holograpic recording is calculated in the far field, the justification of which is discussed in Sec. II E.

The intensities measured, both in direct and in reciprocal holography, consist of three contributions: The square of the primary wave, an interference term, and the square of the scattered waves. In keeping with holographic terminology, the primary wave will henceforth be called the reference wave. For the reconstruction, the interference part is used which preserves the phases of the scattered waves. In contrast, classical crystallographic methods extract structural information from the square of the scattered waves which does not directly reveal absolute phase information.

For small clusters, the square of the reference wave is dominant, the interference term induces a weak angular modulation of the measured intensity and the square of the scattered waves is negligible. As the crystalline cluster becomes larger, constructive interference from the many coherently scattered waves produces strong modulations of the measured intensity in directions which lie on cones around reciprocal lattice vectors $\mathbf{H}$ whose opening angles are $\Theta=\arcsin(|\mathbf{H}|/2k)$. This is the origin of the Kossel lines in the recorded fluorescence. Within a Kossel line, the contribution of the square of the scattered waves to the measured intensity may not be negligible. It must be subtracted from the recorded data to obtain a pure hologram. A possible scheme for doing this is discussed in Sec. II C.

Reconstruction of the hologram is done numerically by a procedure which is essentially a Fourier transform. The information present in one hologram lies on the two-dimensional surface of the Ewald sphere in three-dimensional space. It is therefore incomplete and produces ghost images. In the technique of multiple energy x-ray holography, the ghost images are suppressed by properly phased addition of several reconstructions with different wave numbers,[7] thus extending the Fourier transform to a truly three-dimensional part of reciprocal space. We will discuss this matter from another viewpoint in Sec. II A. We begin our detailed discussion with direct holography of small clusters, proceed to large crystals in the kinematical approximation, discuss the connection with the Kossel technique, look at reciprocal holography, and discuss near-field effects.

A. Direct holography from small clusters

The electric dipole field at point $\mathbf{r}$ from a fluorescent atom at the origin with a dipole moment $\mathbf{p}$ is given by Jackson,[26] Eq. (9.18):

$$\mathbf{E}(\mathbf{r})=k^2\mathbf{p}_{\mathbf{n}'}\frac{e^{ik|\mathbf{r}|}}{|\mathbf{r}|}+[3\mathbf{n}'(\mathbf{n}'\cdot\mathbf{p})-\mathbf{p}]\left(\frac{1}{|\mathbf{r}|^2}-\frac{ik}{|\mathbf{r}|}\right)\frac{e^{ik|\mathbf{r}|}}{|\mathbf{r}|}, \tag{1}$$

where $\mathbf{n}'=\mathbf{r}/|\mathbf{r}|$ is the normal vector in the direction of $\mathbf{r}$ and $\mathbf{p}_{\mathbf{n}'}=\mathbf{n}'\times\mathbf{p}\times\mathbf{n}'$. The second term contains a longitudinal component and is relevant in the near field—which is where the closest neighbor atoms are for typical x-ray wavelengths.

Since multiple scattering is very weak in small clusters, we consider only single scattering. We restrict ourselves to x-ray energies far from any absorption edges of the scattering atoms. The Thomson scattering amplitude measured at point $\mathbf{R}$ due to the field of Eq. (1) from an electron at point $\mathbf{r}$ is given in the far field by Jackson,[26] Eqs. (14.107) and (14.99):

$$\mathbf{E}_{\mathbf{r}}(\mathbf{R})=\frac{e^2}{mc^2}\{\mathbf{n}\times[\mathbf{n}\times\mathbf{E}(\mathbf{r})]\}\frac{e^{ik|\mathbf{R}-\mathbf{r}|}}{|\mathbf{R}-\mathbf{r}|}. \tag{2}$$

Inserting Eq. (1) and writing $\mathbf{k}=k\mathbf{n}$ leads to

$$\mathbf{E}_{\mathbf{r}}(\mathbf{R})=-r_e\frac{e^{ik|\mathbf{R}-\mathbf{r}|}}{|\mathbf{R}-\mathbf{r}|}\frac{e^{ik|\mathbf{r}|}}{|\mathbf{r}|}\times\left[(\mathbf{p}_{\mathbf{n}'})_{\mathbf{k}}+[3\mathbf{n}'(\mathbf{n}'\cdot\mathbf{p})-\mathbf{p}]_{\mathbf{k}}\left(\frac{1}{(k|\mathbf{r}|)^2}-\frac{i}{k|\mathbf{r}|}\right)\right], \tag{3}$$

where $r_e=e^2/mc^2$ is the classical electron radius and $\mathbf{n}=(\mathbf{R}-\mathbf{r})/|\mathbf{R}-\mathbf{r}|$ is the normal vector in the direction of $\mathbf{R}-\mathbf{r}$.

The detector at point $\mathbf{R}$ is in the far field. Since $|\mathbf{r}|\ll|\mathbf{R}|$, we may approximate in Eq. (3) $|\mathbf{R}-\mathbf{r}|^{-1}\approx|\mathbf{R}|^{-1}$ and $\exp(ik|\mathbf{R}-\mathbf{r}|)\approx\exp(ik|\mathbf{R}|-i\mathbf{k}\cdot\mathbf{r})$ with $\mathbf{k}=k\mathbf{R}/|\mathbf{R}|$. The amplitude $\mathbf{E}_D$ at the detector is obtained by taking the far field term of Eq. (1) and adding to it the sum over the scattering from all neighbor atoms at positions $\mathbf{r}_j$ of the emitter of fluorescence. We use $(\mathbf{n}'\times\mathbf{p})\times\mathbf{n}'=\mathbf{p}-(\mathbf{n}'\cdot\mathbf{p})\mathbf{n}'$ to resolve

the multiple vector product $(\mathbf{p}_{\mathbf{n}'})_{\mathbf{k}}$ in Eq. (3), approximate $\mathbf{n}\approx\mathbf{R}/R$ and write $\mathbf{n}'=\mathbf{r}_j/|\mathbf{r}_j|$.

$$\mathbf{E}_D(\mathbf{R})=\frac{e^{ik|\mathbf{R}|}}{|\mathbf{R}|}\left\{\left[\mathbf{p}_{\mathbf{k}}-r_e\sum_j\frac{e^{i(k|\mathbf{r}_j|-\mathbf{k}\cdot\mathbf{r}_j)}}{|\mathbf{r}_j|}f(\mathbf{r}_j,\mathbf{k})\right.\right.$$
$$\times\left[\left(1-\frac{1}{k^2|\mathbf{r}_j|^2}+\frac{i}{k|\mathbf{r}_j|}\right)\mathbf{p}_{\mathbf{k}}\right.$$
$$\left.\left.+\left(\frac{3}{k^2|\mathbf{r}_j|^2}-\frac{3i}{k|\mathbf{r}_j|}-1\right)\frac{(\mathbf{r}_j\cdot\mathbf{p})(\mathbf{r}_j)_{\mathbf{k}}}{|\mathbf{r}_j|^2}\right]\right\},\quad(4)$$

where $f(\mathbf{r}_j,\mathbf{k})$ is the atom form factor for scattering from the direction of $\mathbf{r}_j$ to $\mathbf{k}$. Since it is defined for the scattering of plane waves, its use implies an approximation (see discussion in Sec. II E). The scattering term containing the ratios $r_e/|\mathbf{r}_j|$ is typically smaller than the first one in Eq. (4) by a factor of 10^{-4}–10^{-3}.

The intensity that is recorded by an x-ray detector is a sum of three terms (i) the square of the direct wave, (ii) an interference term, being twice the real part of the product of the direct wave and the scattering term, and (iii) the square of the scattered waves. The latter one is negligible for small clusters. We are then left with terms (i) and (ii). With the abbreviations $A_k(\mathbf{r}_j)=1-(k|\mathbf{r}_j|)^{-2}+i(k|\mathbf{r}_j|)^{-1}$ and $B_k(\mathbf{r}_j)=-2(k|\mathbf{r}_j|)^{-2}+2i(k|\mathbf{r}_j|)^{-1}$, we obtain

$$|\mathbf{E}_D(\mathbf{R})|^2=\frac{1}{R^2}\left\{\left|\mathbf{p}_{\mathbf{k}}\right|^2-2r_e\mathrm{Re}\sum_j f(\mathbf{r}_j,\mathbf{k})\frac{e^{i(k|\mathbf{r}_j|-\mathbf{k}\cdot\mathbf{r}_j)}}{|\mathbf{r}_j|}\right.$$
$$\times\left[A_k(\mathbf{r}_j)|\mathbf{p}_{\mathbf{k}}|^2\right.$$
$$\left.\left.-[A_k(\mathbf{r}_j)+B_k(\mathbf{r}_j)](\mathbf{p}_{\mathbf{k}})\cdot\frac{[(\mathbf{r}_j\cdot\mathbf{p})(\mathbf{r}_j)_{\mathbf{k}}]}{|\mathbf{r}_j|^2}\right]\right\}.\quad(5)$$

We assume the fluorescent radiation to be unpolarized and therefore take the average $\langle|\mathbf{E}(\mathbf{R})|^2\rangle$ of the detected intensity over all orientations of $\mathbf{p}$, i.e., take $(4\pi)^{-1}$ times the integral of $|\mathbf{k}\times\mathbf{p}\times\mathbf{k}|^2$ and $(\mathbf{r}_j\cdot\mathbf{p})(\mathbf{k}\times\mathbf{p}\times\mathbf{k})\cdot(\mathbf{k}\times\mathbf{r}_j\times\mathbf{k})$, respectively, over the coordinates Θ and ϕ in spherical coordinates. They turn out to be $2k^4|\mathbf{p}|^2/3$ and $[k^2|\mathbf{r}_j|^2-(\mathbf{k}\cdot\mathbf{r}_j)^2]k^2|\mathbf{p}|^2/3$, respectively.

Since the hologram is an object in reciprocal space (see Sec. III), we write the detected signal in terms of the wave vector $\mathbf{k}=k\mathbf{R}/|\mathbf{R}|$. After collecting some terms and writing $\cos^2(\mathbf{k},\mathbf{r}_j)=(\mathbf{k}\cdot\mathbf{r}_j)^2/(k|\mathbf{r}_j|)^2$, $\sin^2(\mathbf{k},\mathbf{r}_j)=1-(\mathbf{k}\cdot\mathbf{r}_j)^2/(k|\mathbf{r}_j|)^2$, we arrive at

$$\langle|\mathbf{E}_D(\mathbf{k})|^2\rangle=\frac{2k^4|\mathbf{p}|^2}{3R^2}\left[1-2r_e\,\mathrm{Re}\sum_j\frac{e^{i(k|\mathbf{r}_j|-\mathbf{k}\cdot\mathbf{r}_j)}}{|\mathbf{r}_j|}f(\mathbf{r}_j,\mathbf{k})\right.$$
$$\left.\times\left(A_k(\mathbf{r}_j)\frac{1+\cos^2(\mathbf{k},\mathbf{r}_j)}{2}-B_k(\mathbf{r}_j)\frac{\sin^2(\mathbf{k},\mathbf{r}_j)}{2}\right)\right].\quad(6)$$

The factor $1+\cos^2(\mathbf{k},\mathbf{r}_j)$ is an expected result of polarization averaging but the factor $\sin^2(\mathbf{k},\mathbf{r}_j)$ is a near field effect, coming from the longitudinal component of the fluorescent wave. Furthermore, the near field correction term $i/k|\mathbf{r}_j|$ in $A_k(\mathbf{r}_j)$ and $B_k(\mathbf{r}_j)$ produces a phase shift in the scattered waves. At a recording wavelength of 1.5 Å, its relative weight to the leading order terms is roughly 10% for the nearest neighbor atoms. Since $A_k(\mathbf{r}_j)$ and $B_k(\mathbf{r}_j)$ are multiplied by factors which depend on the angle between $\mathbf{k}$ and $\mathbf{r}_j$, the apparent scattering phase in the polarization-averaged data is anisotropic for the near field.

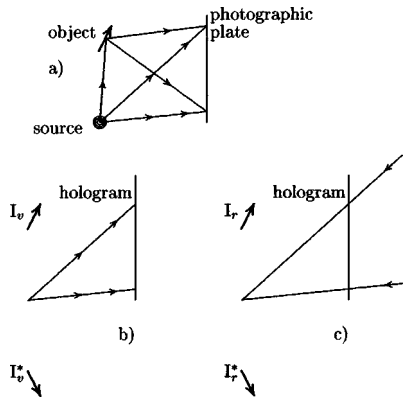

FIG. 1. Lensless Fourier transform holography (a) recording, (b) reconstruction of the virtual image I_v and the conjugate virtual image I_v^* with a diverging illuminating beam, (c) reconstruction of the real image I_r and the conjugate real image I_r^* with a converging illuminating beam.

By introduction of effective scattering form factors $f'(\mathbf{r}_j,\mathbf{k})$, given by $f(\mathbf{r}_j,\mathbf{k})$ times the content of the parentheses following $f(\mathbf{r}_j,\mathbf{k})$ in Eq. (6), this equation may be reduced to the simple form

$$|E_D(\mathbf{k})|^2=\frac{2k^4|\mathbf{p}|^2}{3R^2}\left(1-2r_e\,\mathrm{Re}\sum_j\frac{e^{ik|\mathbf{r}_j|-i\mathbf{k}\cdot\mathbf{r}_j}}{|\mathbf{r}_j|}f'(\mathbf{r}_j,\mathbf{k})\right)\quad(7)$$

which is familiar from derivations of the holographic intensity with scalar waves,[2,24] but with $f(\mathbf{r}_j,\mathbf{k})$ instead of $f'(\mathbf{r}_j,\mathbf{k})$. We must note, however, that due to the factors $\cos^2(\mathbf{k},\mathbf{r}_j)$ and $\sin^2(\mathbf{k},\mathbf{r}_j)$, the effective scattering factor $f'(\mathbf{r}_j,\mathbf{k})$ is generally not physically realizable. Therefore, there is generally no scalar wave equation for the function that leads to the far field amplitude $E_D(\mathbf{k})$.

The second term in Eq. (7), subsequently called $\chi(\mathbf{k})$, contains the holographic information. This information is incomplete because it consists only of the real part of the scattered waves. It can, however, be made complete by combining measurements made at several wave numbers. This has the effect of rotating the phase of the scattering contribution of the atom at $\mathbf{r}_j$ by the factor $\exp(ik|\mathbf{r}_j|)$ contained in it, so that for different wave numbers, different parts of the scattering contribution are projected onto the real axis.

As stated in the Introduction, direct atomic holography is very similar to lensless Fourier transform holography[1] which is shown schematically in Fig. 1. Both the real image and the corresponding ghost image in the above reconstruction of atomic holography are real images in the terminology of holography.

Reconstruction of the hologram is done numerically. We develop here a relatively simple scalar reconstruction for-

mula which essentially involves a reversal of waves. As stated above, this is not perfectly correct because of the lack of a scalar wave equation that would represent the result of polarization averaging of electromagnetic waves. However, we get a workable approximation and obtain a guideline for application of the same ideas to a fully vectorial formalism.

In our scalar formalism, the image that is produced in the reconstruction approximates the field strength that would be present in a sample with scalar scatterers having the above effective scattering factors. The field strength is in turn related to the electron density of the sample.

First, we construct an artificial sample which will turn out to be just what the reconstruction of a real sample images. It is only introduced as a tool for a derivation of the formalism by a simple reversal of waves and not for the reconstruction procedure itself. Furthermore, it will help to understand the nature of the ghost images, the winking effect, and provides a derivation of the reconstruction formalism which does not depend on the Kirchhoff approximation. Since we reconstruct within a scalar wave formalism, we take the scattering form factors $f'(\mathbf{r}_j,\mathbf{k})$ of Eq. (7). Additionally, for each atom at position $\mathbf{r}_j$, we place another atom which we call ''virtual counterpart'' at the position $-\mathbf{r}_j$. It emits a wave with the same angular distribution [given by $f'(\mathbf{r}_j,\mathbf{k})$] as the atom at $\mathbf{r}_j$ and with a relative phase to the fluorescent atom at the origin of not $\exp(ik|\mathbf{r}_j|)$ but rather $\exp(-ik|\mathbf{r}_j|)$. The virtual counterpart of the atom at $\mathbf{r}_j$ is a mathematical construction only. A real atom of the same species which might be sitting at $-\mathbf{r}_j$ would have an atom form factor of $f'(-\mathbf{r}_j,\mathbf{k})$.

We now have the fluorescent spherical wave from the origin, the scattered waves from all really present atoms and the additional, artificially constructed waves. By construction, the amplitudes from the real atoms and from the virtual counterparts add up to the real part of the scattering term in Eq. (7). If we now multiply the detected intensity of Eq. (7) by $3R\exp(ikR)/(2k^2|\mathbf{p}|)$, we get the *amplitude* that our artificial arrangement produces on the sphere of radius R. This is the amplitude that we can use in the reversal of waves of the reconstruction process.

In order to reconstruct the hologram, we calculate the amplitude $\psi_k(\mathbf{r})$ inside a sphere of radius R with an amplitude transmission $1+\chi(\mathbf{r}=R\mathbf{k}/k)$ on which a converging spherical wave $\exp(-ik|\mathbf{r}|)/|\mathbf{r}|$ is incident. The amplitude $\psi_k(\mathbf{r})=[1+\chi(\mathbf{r})]\exp(-ik|\mathbf{r}|)/|\mathbf{r}|$ on the inside of this sphere is then the same as would be found if all waves of our artificial arrangement were reversed (i.e., complex conjugated). Therefore, by Green's theorem, the intensity everywhere inside the sphere is the same as the intensity of the waves emitted in the holographic recording. There is a huge intensity maximum at the origin, corresponding to the emitting atom and further maxima at the positions $\mathbf{r}_j$ of the neighbor atoms and at $-\mathbf{r}_j$, commonly called ghost images, for the virtual counterparts. All of them are smaller than the maximum at the origin by a factor of roughly $f(\mathbf{r}_j)r_e^2/|\mathbf{r}_j|^2$. Because of linear superposition, the maximum at the origin can be suppressed by using $\chi(\mathbf{r})$ instead of $1+\chi(\mathbf{r})$ in the reconstruction.

Commonly,[4] the diffraction pattern of the reconstruction is calculated with the Kirchhoff integral formula, suggesting use of the Kirchhoff approximation with its mathematical inconsistency.[26,27] Our argument with the reversal of waves from the artificial sample shows that the Kirchhoff approximation is not necessary—the result, depending only on the far field approximation $\exp(ik|\mathbf{R}-\mathbf{r}_j|)\approx\exp(ik|\mathbf{R}|-i\mathbf{k}\cdot\mathbf{r}_j)$ which was used for Eq. (4), is almost exact.

The reconstructed wave field, being complex conjugate to the recording wave field from the artificial sample (with the virtual counterparts) is just the complex conjugate of Eq. (4) with the summation extending over all atoms *and* the virtual counterparts (compare to Ref. 4). Specifically, the contribution of an atom at position $\mathbf{a}$ to the reconstructed image has a phase $\exp(-ik|\mathbf{a}|)$ at $\mathbf{a}$ and a phase $\exp(ik|\mathbf{a}|)$ at the position $-\mathbf{a}$ of the virtual counterpart.

If the sample contains atoms at the positions $\pm\mathbf{a}$ then the reconstructed amplitude at $\mathbf{a}$ will have a contribution with phase $\exp(-ik|\mathbf{a}|)$ from the atom at $\mathbf{a}$ and a contribution with phase $\exp(ik|\mathbf{a}|)$ from the virtual counterpart of the atom at $-\mathbf{a}$. These contributions interfere constructively or destructively, depending on $k|\mathbf{a}|$, producing a winking of the sum amplitude in a scan over k.

For a formal calculation of the diffraction pattern of the reversed waves, we use Green's formula. The calculation is carried out in the appendix and results in

$$\psi_k(\mathbf{r})\approx-\frac{i}{2\pi R}\int_S\chi(\mathbf{k})e^{-i\mathbf{k}\cdot\mathbf{r}}d\sigma_k. \tag{8}$$

$d\sigma_k=k/R\ d\sigma$ is now the surface element on the sphere in terms of the coordinate $\mathbf{k}$. As mentioned right after Eq. (6), there is a substantial phase shift in the scattering due to near field effects. This has the effect of a shift of the apparent atom positions in the reconstructed image.

In order to remove the ghost images, we take several reconstructions $\psi_k(\mathbf{r})$ with different wave numbers k and calculate the sum:

$$\psi(\mathbf{r})=\sum_k\ \psi_k(\mathbf{r})e^{-ik|\mathbf{r}|}. \tag{9}$$

In this sum, the phase at the positions of the atoms that were actually present in the recording is stationary because it is being compensated by the factor $\exp(-ik|\mathbf{r}|)$. At ghost image positions, a factor $\exp(-2ik|\mathbf{r}|)$ causes partially destructive interference of the contributions to the sum.[7] Therefore, $\psi(\mathbf{r})$ now represents the electron density with suppressed ghost images. Figure 2 shows this effect in a simulation. Two Cu atoms were put at the positions (3.75 Å,0,0) and (3.75 Å, 3.75 Å,0). Holograms were calculated for the x-ray energies 15,16, . . . ,30 keV according to Eq. (5). The top figure shows a reconstruction with 30 keV according to Eq. (8) for the $z=0$ plane. Ghost images show up at the mirror image positions. For the lower figure, Eq. (9) was used with all sixteen x-ray energies for a reconstruction in the $z=0$ plane. The ghost images are now strongly suppressed.

The image that is obtained in a single energy reconstruction is the complex conjugate of the field strength in the sample, modified by the near field effects which lead to the definition of the effective atomic form factors, and is superimposed with the ghost images.

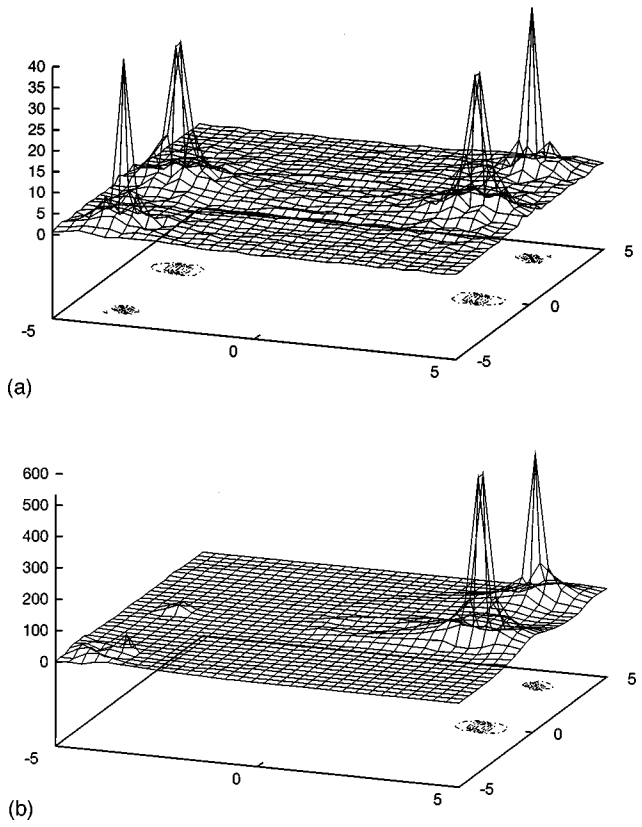

FIG. 2. Comparison of single energy (top) and multiple energy (bottom) x-ray holography in a simulation. The horizontal axes are labeled in Å and the vertical axes, showing $|\psi_k(\mathbf{r})|^2$ (top) and $|\psi(\mathbf{r})|^2$ (bottom) are scaled in arbitrary units. The planes below the grid graphs show contour maps.

B. Kossel lines

As the size of the crystalline cluster grows, Kossel lines appear in the hologram. They are quite sharp and localized which reflects the fact that many atoms at different distances from the origin contribute to the hologram with a wide range of spatial frequencies.

In the Kossel technique, the shape of the Kossel lines is analyzed to obtain phase information.[28–31] To our knowledge, the theory used is always based on the two-beam approximation. Here, we derive a formula in the context of kinematical theory that describes the shape of Kossel lines in a way that inherently does not require any few-beam approximation. For the sake of simplicity, we do the calculations with scalar waves but note that the vectorial nature of electromagnetic waves has an influence on the shape of the Kossel lines.

Far from any absorption edges, there is only Thomson scattering. The sum over the scalar scattering contributions from all atoms in Eq. (4) may then be written in terms of the electron density $\rho(\mathbf{r})$ as

$$s(\mathbf{k})=\sum_j f(\mathbf{r}_j,\mathbf{k})\frac{e^{i(k|\mathbf{r}_j|-\mathbf{k}\cdot\mathbf{r}_j)}}{|\mathbf{r}_j|}=\int_C d^3\mathbf{r}\ \rho(\mathbf{r})\frac{e^{i(k|\mathbf{r}|-\mathbf{k}\cdot\mathbf{r})}}{|\mathbf{r}|}, \tag{10}$$

where C is the volume of the crystal.

The Fourier series of $\rho(\mathbf{r})$ is[19]

$$\rho(\mathbf{r})=\sum_H F_H e^{i\mathbf{H}\cdot\mathbf{r}},\quad F_H=\frac{1}{V}\int_V d^3\mathbf{r}\ \rho(\mathbf{r})e^{-i\mathbf{H}\cdot\mathbf{r}}, \tag{11}$$

where V is the volume of one unit cell and H is the index of the reciprocal lattice vector $\mathbf{H}$.

This gives

$$s(\mathbf{k})=\sum_H F_H\int_C d^3\mathbf{r}\frac{\cos[(\mathbf{k}-\mathbf{H})\cdot\mathbf{r}]e^{ik|\mathbf{r}|}}{|\mathbf{r}|}. \tag{12}$$

The term $\sin(\mathbf{k}-\mathbf{H})\cdot\mathbf{r}$ vanishes due to symmetry.

For C being a sphere around the origin, the integration is easily done in spherical coordinates (r,Θ,ϕ) with $\mathbf{k}-\mathbf{H}$ along the z axis. In the limit of an infinitely large sphere k has to be replaced by $k_c=k+ik_i$ with an imaginary part $k_i>0$. The physical reason for this is that we did not take into account the absorption and extinction of the outgoing unscattered wave. The result is then

$$s(\mathbf{k})=4\pi\sum_H F_H\frac{1}{(\mathbf{k}-\mathbf{H})^2-k_c^2}. \tag{13}$$

In the case of crystalline clusters instead of infinite crystals, the Fourier series is replaced by a Fourier integral, i.e., the sum over H in Eq. (13) is replaced by an integral over $\mathbf{H}$.

For $\mathbf{H}=\mathbf{0}$, Eq. (13) diverges for $k_i\to 0$ for all $\mathbf{k}$. This describes the outgoing, unscattered spherical wave of fluorescent radiation.

For $\mathbf{H}\neq\mathbf{0}$, the denominator in Eq. (13) becomes as small as $-2ik_rk_i+k_i^2$ if $(\mathbf{k}-\mathbf{H})^2=k_r^2$, i.e., if the Bragg condition $\Theta=\arcsin(|\mathbf{H}|/2k)$ is fulfilled. This is the case on a cone around $\mathbf{H}$ with an apex angle of $\pi-2\Theta$, the Kossel cone of $\mathbf{H}$.

The intensity at location $\mathbf{R}$ is then

$$|E(\mathbf{R})|^2$$
$$=\frac{E_0^2R_0^2}{R^2}\left(1+8\pi r_e\ \mathrm{Re}\sum_H F_H\frac{1}{(\mathbf{k}-\mathbf{H})^2-k_c^2}\right.$$
$$\left.+16\pi^2r_e^2\sum_{H,H'}\frac{F_HF_{H'}^*}{[(\mathbf{k}-\mathbf{H})^2-k_c^2][(\mathbf{k}-\mathbf{H}')^2-(k_c^2)^*]}\right), \tag{14}$$

where $E(\mathbf{R})$ is defined as $E(\mathbf{R}=|\mathbf{R}|\mathbf{k}/k)$.

C. Isolating the interference term

In order to get a hologram from the detected intensity, the interference term has to be isolated. Far away from Kossel lines, the square of the scattered waves is much smaller than the interference term so that it is sufficient to simply subtract a constant background. Near the Kossel lines, this is no longer true. Simply cutting the Kossel lines out of the hologram amounts to neglect of holographic information that is contained in the contribution of the interference term to the Kossel lines. A way out of this problem is found by analysis of the shape (more specifically the asymmetry) of the Kossel lines. The interference term in Eq. (14) has a pole of first order and the last term has a pole of second order for $H=H'$. Therefore, the shape of the Kossel line depends on the ratio of Re F_H to $|F_H|^2$ which is determined by the position of the

fluorescing atom (i.e., by definition the origin) relative to the crystal lattice. It also depends on the absorption of the spherical wave of fluorescence which is expressed by k_i.

A fit to the Kossel line belonging to **H** with the parameters Re F_H and $|F_H|^2$ allows us to subtract the contribution of the last term in Eq. (14) to the detected intensity, leaving the pure hologram. We note, however, that this fit requires the exact theoretical shape of the Kossel line which can be obtained only from a vectorial calculation.

The fitting procedure does not require any structural information that is not contained in the holographic recording. The value **H** of the reciprocal lattice vector around which the respective Kossel line is centered is contained in the orientation and opening angle of the Kossel line and Re F_H, $|F_H|^2$ are fit parameters.

D. Reciprocal holography

Most of the discussion of direct holography holds for reciprocal holography as well because the roles of emitter and detector are just reversed. A plane wave $\mathbf{E}_0\exp(-i\mathbf{k}\cdot\mathbf{r})$ is incident on the sample. In the single scattering approximation, the amplitude $\mathbf{E}(\mathbf{k})$ at the origin is a sum of the direct wave and of contributions that were scattered from neighbor atoms. To calculate it, we take an electron at position **r**. The incident wave induces a dipole moment $\mathbf{p}=-r_e k^{-2}\mathbf{E}_0\exp(-i\mathbf{k}\cdot\mathbf{r})$ in it which gives rise to a scattered amplitude at the origin according to Eq. (1) with $\mathbf{n}'=-\mathbf{r}/|\mathbf{r}|$. We decompose $\mathbf{r}\times\mathbf{E}_0\times\mathbf{r}=\mathbf{E}_0-(\mathbf{r}\cdot\mathbf{E}_0)\mathbf{r}$ and form the sum over the scattering contributions from all neighbor atoms by use of the atomic scattering form factors. Neglecting the square of the scattered waves as in Sec. II A, we obtain for the intensity at the origin

$$|\mathbf{E}(\mathbf{k})|^2=|\mathbf{E}_o|^2-2r_e\ \mathrm{Re}\sum_j\frac{e^{i(k|\mathbf{r}_j|-\mathbf{k}\cdot\mathbf{r}_j)}}{|\mathbf{r}_j|}f(\mathbf{r}_j,\mathbf{k})\times\left[A_k(\mathbf{r}_j)|\mathbf{E}_0|^2-(A_k(\mathbf{r}_j)+B_k(\mathbf{r}_j))\frac{(\mathbf{r}_j\cdot\mathbf{E}_0)^2}{|\mathbf{r}_j|^2}\right]. \tag{15}$$

This equation describes the reciprocal hologram for fully polarized incident radiation. In order to compare this result to Eq. (6), we take the average $\langle|\mathbf{E}(\mathbf{k})|^2\rangle$ over all possible polarizations. Contrary to Sec. II A, this average extends not over a sphere but only a circle around **k**, for each **k** separately. The averages over $|\mathbf{E}_0|^2$ are trivial and the average over $(\mathbf{E}_0\cdot\mathbf{r}_j)^2$ gives $|\mathbf{r}_j|^2|\mathbf{E}_0|^2\sin^2(\mathbf{k},\mathbf{r}_j)/2$. We have now

$$\langle|\mathbf{E}(\mathbf{k})|^2\rangle=|\mathbf{E}_0|^2\left[1-2r_e\ \mathrm{Re}\sum_j\frac{e^{i(k|\mathbf{r}_j|-\mathbf{k}\cdot\mathbf{r}_j)}}{|\mathbf{r}_j|}f(\mathbf{r}_j,\mathbf{k})\times\left(A_k(\mathbf{r}_j)\frac{1+\cos^2(\mathbf{k},\mathbf{r}_j)}{2}-B_k(\mathbf{r}_j)\frac{\sin^2(\mathbf{k},\mathbf{r}_j)}{2}\right)\right] \tag{16}$$

which—except for a scaling factor—is just the same as Eq. (6). Therefore, the reconstruction procedure that was derived in Sec. II A may be used for reciprocal holography with unpolarized incident radiation, too.

A reconstruction formula which is based on the reversal of waves may be found by application of the concept of the virtual counterparts, as described in Sec. II A if the polarization of the incident radiation is chosen to depend on the incident direction in a way which is reciprocal to direct holography from a polarized (i.e., not polarization-averaged) source. This work is yet to be done quantitatively. Some initial work[25] has been published on the visibility of atoms in different directions with respect to the polarization.

E. Near field effects

We have used (i) the far field approximation in the derivation of Eq. (4) by replacing the spherical wave that goes out to the detector from the scattering atoms by a plane wave. Furthermore, (ii) the spherical wave $\exp(ik|\mathbf{r}_j|)/|\mathbf{r}_j|$ in Eq. (4) and taking the intensity only in the origin in Eq. (15) implies the assumption that the fluorescent atom in the origin be pointlike. Finally, (iii) in the derivation of Eqs. (4) and (15), we assumed pointlike scatterers.

Our assumption (i) actually depends on the solid angle of the active detector area: The smaller it is, the better justified is assumption (i). In direct holography, assumption (ii) is justified if the spatial extent of the atomic orbitals that are participating in the x-ray fluorescence is much smaller than interatomic distances—a condition which is almost always very well satisfied.

Assumption (iii) is valid for the scattering of plane waves by introduction of atomic scattering factors. In our case, however, the incoming wave in direct holography or the scattered wave in reciprocal holography is spherical. Therefore, the tabulated values of the scattering factors are somewhat inaccurate, depending on how strongly curved the spherical wave is within the electron cloud of the scattering atom.

There are some pronounced near field effects which have their origin in the vectorial nature of electromagnetic waves. They lead to the correction terms which decrease as $i/k|\mathbf{r}_j|$ and $1/k^2|\mathbf{r}_j|^2$ as compared to the leading order in Eqs. (6) and (15). Furthermore, direct and reciprocal holography differ in these correction terms and are therefore not exactly equivalent.

III. ATOMIC HOLOGRAPHY IN RECIPROCAL SPACE

The holographic data is obtained from the surface of the Ewald sphere which is centered at the origin of reciprocal space and whose radius is given by the wave number. Figure 3 shows the transition from an infinite lattice to a cluster. The infinite lattice has Fourier components located at points in reciprocal space. For each reciprocal lattice vector, there is a Kossel line which is a circle on the Ewald sphere and is the locus of all wave vectors which fulfil the Bragg condition for the respective reciprocal lattice point.

As the sampled volume becomes smaller, the Fourier series of Eq. (11) has to be replaced by a Fourier integral, i.e., the reciprocal lattice points become spread out. Correspondingly, the Kossel lines are smeared out. As the cluster becomes very small, the Kossel lines disappear and there is a weak modulation of the intensity all over the Ewald sphere.

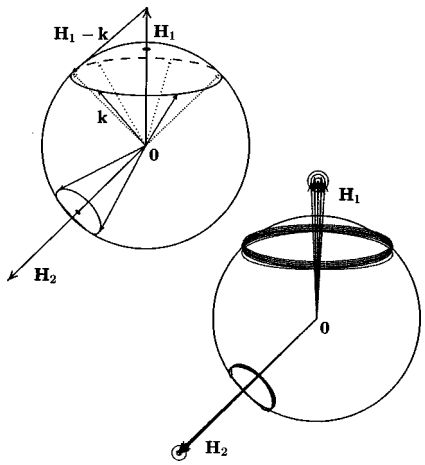

FIG. 3. The Ewald sphere in reciprocal space. Left: An infinite lattice, two reciprocal lattice vectors $\mathbf{H}_1$, $\mathbf{H}_2$, their Kossel lines and one Bragg reflex from $\mathbf{k}$ to $\mathbf{H}_1-\mathbf{k}$. Right: A cluster, the reciprocal lattice points and the Kossel lines become smeared out.

IV. EXPERIMENT

The theory was tested by measurements in the multiple energy mode because it has a good angular resolution and provides a possibility of wide parameter variation. The experiments were carried out with synchrotron radiation at HASYLAB on beamlines BW1 and CEMO. A Si(111) double crystal monochromator provided a monochromatic collimated incident beam with energies from 9 to 30 keV and $\Delta E/E \sim 10^{-4}$. A flat polished single crystal of Cu_3Au was mounted on a four-circle goniometer to provide rotation by the incidence angles Θ (inclination, measured from the surface) and ϕ (azimuth) over a wide angular range. Energy dispersive silicon drift detectors[32,33] with an energy resolution of 300 eV at 10 keV and counting rates of 2×10^5 s^{-1} were used to register separately fluorescent radiation in the Cu K_α and Au L lines. The technique of multiple energy x-ray holography was applied in a modified way, as the detectors kept a constant angle to the sample surface, but did not follow the azimuthal rotation ϕ of the sample.

Figure 4 shows an experimental hologram, recorded with Cu K_α radiation at an incident energy of 24 keV. The background from the reference wave was removed and corrections for absorption were applied. Kossel lines, belonging to Bragg diffraction of the incident radiation are clearly visible. Due to beamtime limitations, the density of data points was too low to allow a separation of the contributions to the Kossel lines as described in Sec. II C. However, far from the Kossel lines the contrast may be attributed to the linear interference term in Eq. (4) alone and is consequently evaluated in the holographic approach.

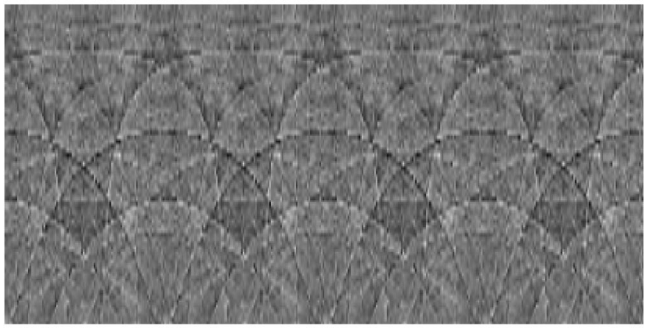

FIG. 4. A hologram of Cu_3Au with Kossel lines. Horizontal axis: $\phi=0°,1°,\ldots,360°$; vertical axis: $\Theta=19°,20°,\ldots,90°$.

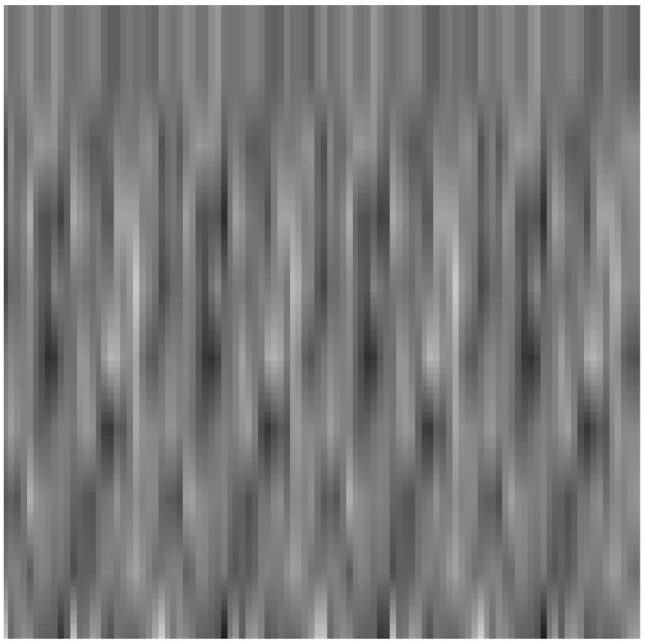

FIG. 5. A hologram of Cu_3Au with lower resolution than in Fig. 4. Horizontal axis: $\phi=0°,1°,\ldots,360°$; vertical axis $\Theta=45°,50°,\ldots,85°$. The data was symmetrized to four-fold symmetry.

The hologram of Fig. 5 was measured at 9.35 keV with an angular step size which was five times larger in the Θ direction than in Fig. 4. The large step size served as a low pass filter and excluded the high frequency Bragg scattering components. A reconstruction of the hologram in the base plane of the Cu_3Au face centered cubic lattice cell is shown in Fig. 6. The central detecting copper atom is excluded from the reconstructed image by the reconstruction procedure according to Eq. (8), integrating only over that part of the sphere on which holographic data was taken.

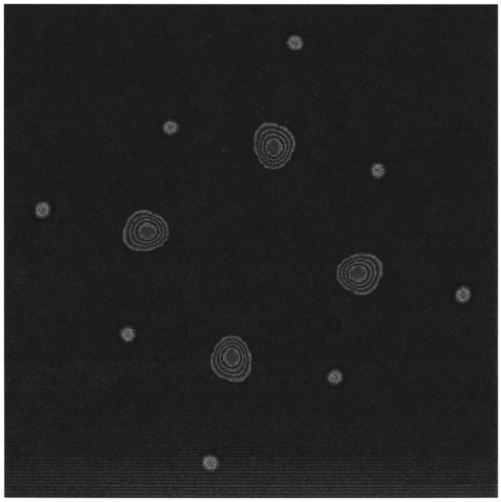

FIG. 6. Reconstruction from the hologram of Fig. 5. The smaller and larger spots are at the positions of Cu and Au, respectively.

The nearest neighbors of the detecting Cu atoms are Au and the next nearest neighbors are Cu. Au atoms, having more than twice as many electrons than Cu, produce much more pronounced maxima in the reconstructed image.

V. DISCUSSION

X-ray holography with atomic resolution provides an x-ray optical image of the atomic short range order. The formalism developed here also includes long range order by way of the Kossel lines. Thus, the holographic interpretation of scattering data avoids the phase problem of crystallography. The emphasis of atomic holography as presented here is on the immediate atomic neighborhood of the fluorescing atoms. This application requires interference information from a large solid angle with moderate angular resolution. As evident from the exponent in Eq. (7), the spatial frequency of the contribution of a scattering atom to the interference pattern scales with its distance from the origin. Therefore, the angular resolution required depends on the spatial range of the reconstruction. Since all atoms of a large crystal contribute to the interference pattern with their respective spatial frequencies, the Kossel lines are sharp and localized. In the case of a large crystal, the square of the scattered waves which was neglected in Eq. (5), becomes noticeable. It then becomes possible to determine the position of the fluorescing atom relative to the crystal lattice by analysis of the shape of the Kossel lines as given by Eq. (14). This leads to the methods of standing waves and standing waves in reverse which are the limiting cases of reciprocal and direct holography, respectively.

The standing wave method is usually done in the context of dynamical scattering theory, as is appropriate to large perfect crystals. If the crystal is large but not quite so perfect—or slightly off the Kossel lines—the result (14) which was developed in the kinematical approximation is valid. The phase angle $\arctan(\mathrm{Re}\, F_H/|F_H|)$ which can be obtained by a fit to the shape of the Kossel line belonging to the reciprocal lattice vector **H** as described in Sec. II C is the direct analog to the coherent position of the standing wave method.

It is important to realize that the reconstruction formula that was derived in Sec. II A does not give an image of the electron density. It rather returns an image that is related to the electrical wave field in the sample at recording time, being the complex conjugate of the wave field amplitude in the auxiliary sample that was constructed in Sec. II A as a tool for the derivations. A full reconstruction of the electron density will require further steps: first corrections for the influence of the near field terms, such as the apparent shift of the atom positions, described in Sec. II A and then a procedure to obtain the electron density from the amplitude of the scattered waves inside the sample. This will certainly require multiple energy x-ray holography to probe the atomic scattering form factors at different momentum transfers for constant scattering angle.

VI. CONCLUSIONS

We have discussed both direct and reciprocal x-ray holography in an intuitively appealing way and including polarization and near-field effects, have shown the relation of x-ray holography to crystallography using Bragg reflections. We have also derived a compact formula for Kossel lines in the kinematical approximation. This allows a separation of the contributions to the Kossel lines which belong into the hologram. Our holograms from a crystal of Cu_3Au show clear evidence of Kossel lines.

The hologram obtained experimentally is in good agreement with the theory that was developed in this text. The evaluation of experimental results from single crystals will be discussed in a forthcoming paper.[34]

ACKNOWLEDGMENTS

The authors are indebted to P. M. Len and V. Kaganer for valuable discussions and especially acknowledge the inspiration from discussions with F.N. Chukhovskii and his comments on the manuscript.

APPENDIX: HOLOGRAPHIC RECONSTRUCTION

We insert a modulated converging spherical wave $[1+\chi(\mathbf{r}')]\exp(-ikR)/R$ with $\chi(\mathbf{r}')$ defined as $\chi[\mathbf{k}=k\mathbf{r}'/R)]$ and the Green's function $\phi(\mathbf{r}-\mathbf{r}')=\exp(ik|\mathbf{r}-\mathbf{r}'|)/4\pi|\mathbf{r}-\mathbf{r}'|$ [see Jackson,[26] Eq. (9.122)] into Green's formula to obtain an expression for the amplitude $\psi_k(\mathbf{r})$ at a point $\mathbf{r}$ inside the sphere. Since $\chi(\mathbf{k})$ depends only on the direction and not the distance from the origin, the radial component of $\nabla\chi$ vanishes and we are left with

$$\psi_k(\mathbf{r})=-\frac{1}{4\pi}\int_S[1+\chi(\mathbf{r}')]\frac{e^{ik|\mathbf{r}-\mathbf{r}'|}}{|\mathbf{r}-\mathbf{r}'|}\frac{e^{-ik|\mathbf{r}'|}}{|\mathbf{r}'|}\mathbf{n}' \times\left[\left(ik+\frac{1}{|\mathbf{r}'|}\right)\frac{\mathbf{r}'}{|\mathbf{r}'|}+\left(ik-\frac{1}{|\mathbf{r}-\mathbf{r}'|}\right)\frac{\mathbf{r}-\mathbf{r}'}{|\mathbf{r}-\mathbf{r}'|}\right]d\sigma. \tag{A1}$$

$\mathbf{r}'$ is on the sphere, $\mathbf{n}'$ is the *inward* surface normal vector of the spherical integration surface, i.e., $\mathbf{n}'\cdot\mathbf{r}'=-|\mathbf{r}'|=-|\mathbf{R}|$, and $d\sigma$ is the surface element on the sphere in terms of the coordinate $\mathbf{r}'$. Since we are interested in the values of ψ_k near the origin, we can make use of some simplifications which are similar to those made before Eq. (4) and

$$\frac{e^{ik|\mathbf{r}-\mathbf{r}'|}}{|\mathbf{r}-\mathbf{r}'|}\approx\frac{e^{ikR}e^{-i\mathbf{r}\cdot\mathbf{k}}}{R},\quad \mathbf{n}'\cdot(\mathbf{r}-\mathbf{r}')\approx R,$$

$$ik-\frac{1}{|\mathbf{r}-\mathbf{r}'|}\approx ik,\quad ik+\frac{1}{|\mathbf{r}'|}\approx ik. \tag{A2}$$

In order to suppress the huge maximum at the origin which is just the focus of the converging spherical wave, we use $\chi(\mathbf{k})$ instead of $1+\chi(\mathbf{k})$ and obtain now

$$\psi_k(\mathbf{r})\approx-\frac{i}{2\pi R}\int_S\chi(\mathbf{k})e^{-i\mathbf{k}\cdot\mathbf{r}}d\sigma_k. \tag{A3}$$

[1] H. A. Smith, *Principles of Holography* (Wiley, New York, 1969).
[2] A. Szöke, in *Short Wavelength Coherent Radiation: Generation and Applications*, edited by T. Atwood and J. Boker, AIP Conf. Proc. No. 147 (AIP, New York, 1986), p. 361.
[3] E. Wolf, Opt. Commun. **1**, 153 (1969).
[4] J. J. Barton, Phys. Rev. Lett. **61**, 1356 (1988).
[5] D. K. Saldin, G. R. Harp, B. L. Chen, and B. P. Tonner, Phys. Rev. B **44**, 2480 (1991).
[6] S. Thevuthasan, G. S. Herman, A. P. Kaduwela, R. S. Saiki, Y. J. Kim, W. Niemczura, M. Burger, and C. S. Fadley, Phys. Rev. Lett. **67**, 469 (1991).
[7] J. J. Barton, Phys. Rev. Lett. **67**, 3106 (1991).
[8] S. Y. Tong, H. Li, and H. Huang, Phys. Rev. Lett. **67**, 3102 (1991).
[9] L. J. Terminello, J. J. Barton, and D. A. Lapiano-Smith, Phys. Rev. Lett. **70**, 599 (1993).
[10] M. Zharnikov, M. Weinelt, P. Zebisch, M. Stichler, and H.-P. Steinrück, Phys. Rev. Lett. **73**, 3548 (1994).
[11] M. Tegze and G. Faigel, Europhys. Lett. **16**, 41 (1991).
[12] T. Gog, P. M. Len, G. Materlik, D. Bahr, C. S. Fadley, and C. Sanchez-Hanke, Phys. Rev. Lett. **76**, 3132 (1996).
[13] P. M. Len, S. Thevutasan, C. S. Fadley, A. P. Kaduwela, and M. A. Van Hove, Phys. Rev. B **50**, 11 275 (1994).
[14] W. Kossel, V. Loeck, and H. Voges, Z. Phys. **94**, 139 (1935).
[15] M. v. Laue, Ann. Phys. (Leipzig) **26**, 55 (1936).
[16] A. M. Afanas'ev *et al.*, Acta Crystallogr., Sect. A: Found. Crystallogr. **A41**, 227 (1985).
[17] S. R. Andrews and R. A. Cowley, J. Phys. C **18**, 6427 (1985).
[18] I. K. Robinson, Phys. Rev. B **33**, 3830 (1986).
[19] M. Bedzyk and G. Materlik, Phys. Rev. B **32**, 6456 (1985).
[20] T. Gog, D. Bahr, and G. Materlik, Phys. Rev. B **51**, 6761 (1995).
[21] D. Gabor, Nature (London) **161**, 777 (1948).
[22] A. Tonomura, Adv. Phys. **41**, 59 (1992).
[23] M. Howells, C. Jacobsen, J. Kirz, R. Feder, K. McQuaid, and S. Rothman, Science **238**, 514 (1987).
[24] P. M. Len, T. Gog, D. Novikov, G. Materlik, and C. S. Fadley, Phys. Rev. B **55**, R3323 (1997).
[25] P. M. Len, C. S. Fadley, and G. Materlik, in *X-Ray and Inner-Shell Proceses*, Proceedings of the 17th International Conference, edited by R. L. Johnson, B. F. Sonntag, and H. Schmidt-Bocking, AIP Conf. Proc. No. **389** (AIP, New York, 1997), p. 295.
[26] J. D. Jackson, *Classical Electrodynamics* (Wiley, New York, 1975).
[27] A. Sommerfeld, *Optics* (Academic, New York, 1964).
[28] J. M. Cowley, Acta Crystallogr. **17**, 33 (1964).
[29] J. P. Hannon and G. T. Trammell, in *Mössbauer Effect Methodology*, edited by I. J. Gruverman, C. W. Seidel, and D. K. Dieterly (Plenum, New York, 1974), Vol. 9.
[30] D. Stephan, and V. Geist, Exp. Tech. Phys. (Berlin) **34**, 153 (1986).
[31] J. T. Hutton, G. T. Trammell, and J. P. Hannon, Phys. Rev. B **31**, 743 (1985).
[32] RÖNTEC, Rudower Chaussee 6, D-12489 Berlin, Germany.
[33] P. Lechner *et al.*, Nucl. Instrum. Methods Phys. Res. A **377**, 346 (1996).
[34] D. V. Novikov, B. Adams, T. Hiort, E. Kossel, and G. Materlik, J. Synchrotron Radiat. (to be published).